Measurement of Gyroid Single Grain Growth Rates in Block Copolymer Solutions

Thomas Q. Chastek and Timothy P. Lodge*

Department of Chemistry, University of Minnesota, Minneapolis, Minnesota 55455-0431

Received June 18, 2003; Revised Manuscript Received July 30, 2003

ABSTRACT: The kinetics of grain growth during thermally induced phase transitions between two block copolymer ordered phases have been determined by polarized optical microscopy (POM). Measurements were made on poly(styrene-*b*-isoprene) copolymers, $f_{PS} = 0.3-0.6$, in solutions with dialkyl phthalates at polymer volume fractions of 0.5−0.7. When these solutions are cooled from a disordered state, they exhibit a transition from the transient metastable hexagonally perforated layer (HPL) phase to the gyroid (G) phase. The HPL to G transition typically occurs through classical nucleation, with radially symmetric grain growth, making it a model system for quantifying the growth front velocities of individual G grains. Temperature jump experiments monitored with POM were used to determine the effect of quench depth on the grain growth rates. Grain growth rates are compared quantitatively to the theoretical predictions of Goveas and Milner, with good agreement observed.

Introduction

Block copolymer order−order phase transitions (OOT) have been identified in many systems. For example, melt block copolymers exhibit the following OOTs: body-centered-cubic array of spheres (BCC) ↔ hexagonally packed cylinders (C), lamellae (L) ↔ gyroid (G), C ↔ G, and C ↔ L.[1,2] Epitaxial mechanisms for several OOTs have been identified, and for both the L → G and C → G, the transition mechanisms often involve the metastable intermediate hexagonally perforated layers phase (HPL).[3−7] Thus, characterizing the HPL → G is relevant to several transitions. Furthermore, the kinetics of block copolymer OOTs have not been thoroughly explored, although some experimental kinetic measurements of OOT have been made.[7−14] Similarly, there have been several studies of ordering kinetics upon quenching from the disordered state through the order−disorder transition (ODT),[15−21] but a complete picture has yet to emerge.

Bates and Rosedale measured the ordering kinetics of several ordered phases through characterization of the elastic modulus.[15] They were able to assign Avrami exponents to the ordering rates and to conclude that grain nucleation was heterogeneous. Singh et al. measured the ordering kinetics of the BCC phase using time-resolved small-angle X-ray scattering (SAXS).[16] From Avrami fits they observed nucleation and growth in the early stages of ordering, followed by grain impingement at late stages of conversion. Sakamoto and Hashimoto characterized lamellar ordering using transmission electron microscopy and time-resolved SAXS.[20] They observed homogeneous nucleation and anisotropic grain growth.

Ordered phases forming in the absence of any external field often do so through formation of distinct grains. Understanding of grain growth mechanisms and kinetics during OOTs and ODTs is important for describing structural and processing features of these block copolymer systems. For example, Balsara et al. measured grain growth kinetics for ordering of the cylinder phase in poly(styrene-*b*-isoprene)s using time-resolved depolarized light scattering.[22−28] They were able to compare their experimental findings to theoretical predictions of Goveas and Milner,[29] who had derived a relationship for the growth front propagation of an individual grain based on several experimentally quantifiable parameters. Balsara et al. found the temperature dependence of their experimentally measured grain growth rates to be in good agreement with the theoretical predictions.

The phase behavior of several poly(styrene-*b*-isoprene)s in a series of dialkyl phthalate solvents has been characterized previously using SAXS and rheology, and many OOTs have been located.[30−32] The dialkyl phthalates preferentially swell the polystyrene microdomains, which alters the effective block composition fraction. Thus, these solvents allow for manipulation of poly(styrene-*b*-isoprene) phase behavior. Furthermore, increased temperature reduces the polystyrene selectivity of the dialkyl phthalates, which gives rise to a larger array of temperature-induced phase sequences than seen in the melt state. In this work we employ polarized optical microscopy (POM) to obtain 2-D images of selected samples during the OOT in real time. This technique is, of course, very familiar in the fields of polymer crystallization and surfactancy[33,34] but has been exploited relatively infrequently for block copolymers.[35−38] The HPL → G transition provides the main focus of this research, since it adheres to a mechanism of nucleation with radially symmetric growth. The individual grain growth behavior and kinetics were measured in detail for six different solutions, and the grain growth velocities were compared to predictions based on the model of Goveas and Milner.[29]

Experimental Section

Samples and Solutions. The synthesis and characterization of four poly(styrene-*b*-isoprene) diblock copolymers, denoted SI(22−12), SI(15−13), SI(8−7), and SI(11−32), have been described elsewhere;[30] the numbers indicate the block molecular weights in kg/mol. The polymers were examined in solutions with the styrene-selective solvents dibutyl phthalate (DBP), diethyl phthalate (DEP), or dimethyl phthalate (DMP), at polymer volume fractions between $\phi = 0.50$ and 0.70. The solvents and polymer concentrations for each sample are listed in Table 1. The solutions were prepared by dissolving polymer and solvent with methylene chloride as a cosolvent, which was then removed under a gentle flow of nitrogen. Less than 0.2

10.1021/ma034833w CCC: $25.00
Published on Web 09/11/2003

Table 1. Properties of the Measured Solutions

	f_{PS}[a]	phase behavior	$\langle h^2\rangle^{1/2}$, Å[b]	N[c]	α[d]
SI(22−12) $\phi = 0.70$ DEP	0.61	G/DIS, 163 °C	123	348	0.1
SI(22−12) $\phi = 0.70$ DBP	0.61	G/DIS, 115 °C	123	348	0.25
SI(8−7) $\phi = 0.64$ DMP	0.49	G/DIS, 95 °C	82	155	1
SI(15−13) $\phi = 0.55$ DEP	0.50	G/DIS, 116 °C	111	285	1
SI(15−13) $\phi = 0.57$ DBP	0.50	G/DIS, 45.2 °C	111	285	2.3
SI(11−32) $\phi = 0.67$ DBP	0.23	G/C, 74 °C	141	456	0.05

[a] Polystyrene volume fraction. [b] Root-mean-square chain end-to-end distance. [c] Degree of polymerization. [d] Experimental scaling factor (used in eq 1).

Table 2. Homopolymers Used To Estimate τ_1 for Diblock Solutions

	homopolymers used to estimate τ_1
SI(22−12) $\phi = 0.70$ DEP	PS-34 $\phi = 0.70$, PI-22 $\phi = 0.70$
SI(22−12) $\phi = 0.70$ DBP	PS-34 $\phi = 0.70$, PI-22 $\phi = 0.70$
SI(15−13) $\phi = 0.55$ DEP	PS-25 $\phi = 0.55$, PI-22 $\phi = 0.55$
SI(15−13) $\phi = 0.57$ DBP	PS-25 $\phi = 0.55$, PI-22 $\phi = 0.55$
SI(8−7) $\phi = 0.64$ DMP	PS-10 $\phi = 0.64$, PI-22 $\phi = 0.64$
SI(11−32) $\phi = 0.67$ DBP	PS-34 $\phi = 0.70$, PI-22 $\phi = 0.70$

wt % 2,6-di-*tert*-butyl-4-methylphenol (BHT) was added to the solutions as an antioxidant. Solutions were stored at −20 °C until use.

All of the samples with the exception of SI(11−32)/DBP exhibited the same equilibrium phase sequence upon cooling: disordered state (DIS) → G → C. For a single quench below T_{ODT} into G, the transition sequence DIS → (HPL) → G was consistently observed. The samples were annealed at 5−10 °C above T_{ODT} prior to quenching, and each prepared sample was used only once to avoid any solvent loss. The phase behavior of SI(11−32)/DBP differed from the other samples: DIS → C → G upon cooling. The transition of interest in this sample was a C → (HPL) → G transition, where the HPL phase forms during sufficiently deep quenches below the C/G phase boundary.[4,7] The C phase was formed by quenching from disorder, first 10 °C below T_{ODT}, and then raising to 5 °C below T_{ODT} after C grain nucleation. Thus, a highly birefringent C phase was formed having typical grain sizes of ca. 25−40 μm.

Rheological measurements were made on disordered solutions of polyisoprene and polystyrene homopolymers denoted PI-22, PS-10, PS-25, and PS-34 to obtain estimates of the longest relaxation times (τ_1) of the copolymer solutions in the absence of microphase separation. PI-22 (93% 1−4 microstructure) was synthesized via living anionic polymerization following the same procedure as the diblocks, except that the reaction was terminated with ethylene oxide before addition of acidic methanol, which resulted in a hydroxyl end group. Characterization by size-exclusion chromatography gave $M_w/M_n = 1.03$ and $M_w = 2.2 \times 10^4$ g/mol. PS-10 was purchased from Polymer Laboratories (batch no. 20129-8) with $M_w/M_n = 1.02$ and $M_w = 1.0 \times 10^4$ g/mol. PS-25 was purchased from Pressure Chemical (lot no. 30811) with $M_w/M_n = 1.06$ and $M_w = 2.5 \times 10^4$ g/mol. PS-34 corresponds to National Institute of Standards and Technology (NIST) standard reference material (SRM) 1478, with $M_w/M_n = 1.01$ and $M_w = 3.4 \times 10^4$ g/mol. Except for PS-34, each of the homopolymers was dissolved in the neutral solvent bis(2-ethylhexyl)phthalate (dioctyl phthalate, DOP) following the same procedure as the copolymers. PS-34 was combined with DOP using benzene as cosolvent, which was removed under vacuum while frozen at 0 °C. The PS-34 and PS-25 solutions were annealed at 100 °C for 2 h before measurements. The homopolymer solutions used to approximate each diblock sample are listed in Table 2. Homopolymers were chosen with similar molecular weights to the diblocks in order to best estimate the copolymer behavior.

All of the dialkyl phthalates were purchased from Aldrich. DEP and DMP were used as received. However, since DBP and DOP had been stored for a sufficiently long interval for some hydrolysis to occur, they were purified by washing with 5% aqueous sodium bicarbonate followed by repeated washing with distilled water. They were dried with calcium chloride for 1−2 days to remove any remaining water.

Polarized Optical Microscopy (POM). POM was used to distinguish between birefringent (L, C, or HPL) and isotropic (DIS, G, or S) phases and to observe grain growth in real space. The measurements were made with a Nikon Optiphot-Pol optical microscope by placing the sample between a vertical polarizer and a horizontal analyzer. Since weakly birefringent samples were measured, a $\lambda/20$ plate was inserted between the polarizer and the sample to enhance the image contrast. Samples in isotropic states did not depolarize the light, and only the waveplate depolarized intensity was transmitted through the analyzer. Birefringent regions either added or subtracted to the waveplate depolarized intensity, resulting in isotropic regions having a uniform gray color, while birefringent regions exhibited either lighter or darker shades. The samples were pressed between two glass coverslips to a thickness of 100−150 μm and sealed with silicone glue. An aluminum sample holder with viewing window connected to a Fenwal 921 temperature controller allowed the sample temperature to be controlled from ambient to 250 °C with an accuracy of ±0.2 °C. The temperature was monitored by a calibrated resistance temperature detector (RTD), and the temperature equilibrated within at most 2 min after a temperature jump.

Small-Angle X-ray Scattering (SAXS). SAXS was used to confirm the phase assignments for the isotropic and birefringent phases observed by POM. A 2 m 2-D SAXS instrument with Cu Kα X-rays ($\lambda = 1.54$ Å) generated by a Rigaku RU-200BVH rotating anode was used, as described elsewhere.[30] The samples were placed in a liquid cooled heating block with a temperature range of 0−200 °C. The sample chamber had a continuous flow of helium, while the alignment optics and flight tube were under vacuum. The images were corrected for detector response. Samples were prepared by pressing the solutions between Kapton films to a thickness of 1−1.5 mm and sealing with silicone glue.

Rheology. Rheological characterization was performed on an ARES instrument (Rheometric Scientific), using 25 mm parallel plates with gap widths of 0.7−2 mm. Relaxation times were determined by measuring the frequency dependence of the dynamic moduli at fixed temperature. The strain amplitude was kept low enough to remain in the linear viscoelastic regime. Since the solutions were not sealed and the temperature was controlled by a nitrogen convection oven, higher temperature measurements were repeated to ensure that solvent loss did not affect the results.

Results and Discussion

The kinetics of individual grain growth were characterized using polarizing optical microscopy (POM). POM measurements were made on the six samples listed in Table 1: SI(22−12)/DEP, SI(22−12)/DBP, SI(15−13)/DEP, SI(15−13)/DBP, SI(8−7)/DMP, and SI(11−32)/DBP. POM was well suited since it could be used to gain 2-D real time images of transitions over a wide range of temperatures and transition rates.

The measurements on all of the samples are in good qualitative agreement. Thus, the transition behavior of all the samples can be illustrated by a representative sample: SI(22−12)/DEP. However, it is important to note that there was substantial quantitative variation in transition rates, nucleation density, and the level of HPL birefringence. Moreover, even though the equilibrium phase behavior of SI(11−32) was different from the other samples, its kinetic behavior was nonetheless in qualitative agreement. These issues will be discussed further subsequently.

All of the samples, except SI(11−32)/DBP, exhibited a DIS → (HPL) → G → C phase transition sequence upon cooling. The HPL phase is both metastable and transient, occurring for some time interval during the

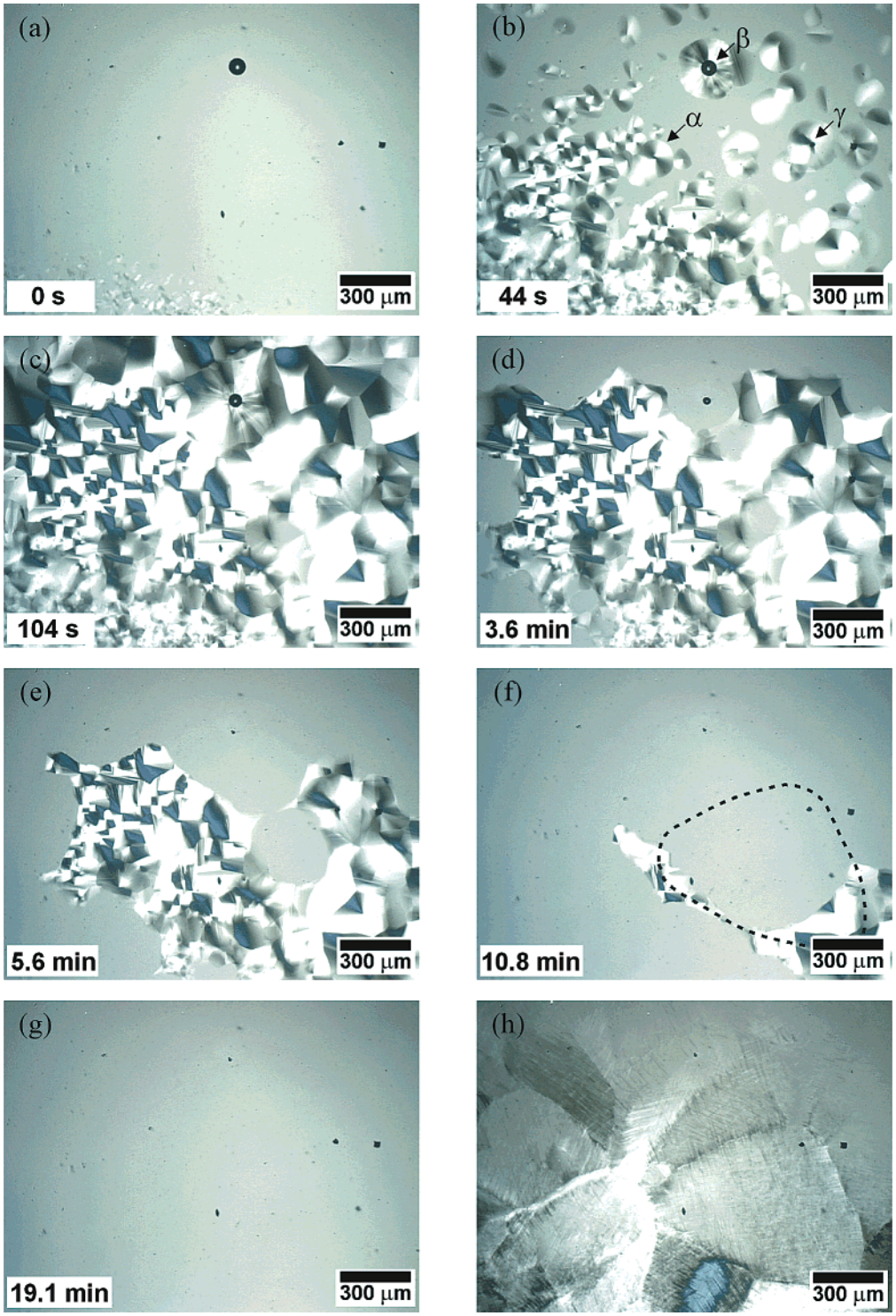

Figure 1. Measurement of SI(22−12) $\phi = 0.7$ in DEP after a temperature quench to 153 °C. (a−c) The isotropic disordered phase transforms to the birefringent HPL. (d−g) After continued measurement at 153 °C, the birefringent HPL transforms to the isotropic G. (h) Measurement 71 min after a further quench to 105 °C shows G partially transforms to C. The outline of a C grain is drawn in the G (f) to highlight the correspondence of G and C grain boundaries.

transition between DIS and G. Thus, quenching to a single temperature below T_{ODT} within G allowed for characterization of the DIS → (HPL) → G transition sequence. A subsequent temperature quench was required to examine the G → C transition. Figure 1a−g shows a sequence of POM images taken on SI(22−12)/DEP after a quench from DIS to 153 °C (G phase region). The resolution and field of view were fixed in all the frames in Figure 1. The sample had been quenched from 190 °C, which is above T_{ODT} (163 °C), and thus the sample was initially isotropic (DIS, Figure 1a). HPL formation can be readily observed in Figure 1b, 44 s after the quench. Figure 1c shows that the HPL phase fills the field of view in under 2 min. The HPL phase then recedes in favor of an isotropic state in Figure 1d−g, as the metastable HPL phase converts to the thermodynamically stable G phase. After G formation was complete (Figure 1g, 19 min after the quench), a second temperature quench to 105 °C was performed, which is below T_{OOT} (130 °C) for the G → C transition.

Figure 1h shows partial formation of the birefringent C phase 71 min after the second temperature quench.

Further inspection of the POM images allowed more detailed aspects of grain formation to be observed. The HPL phase forms from DIS via spherulitic growth. A clear example of a spherulite is denoted by α in Figure 1b. Normally, spherulites observed by POM are dark with a bright central Maltese cross pattern. However, since a partial waveplate was used, the upper-left and lower-right quadrants are dark while the other quadrants are lighter. The nucleation of HPL is at least partially heterogeneous, as evidenced by the visible nucleating agents of a bubble, denoted β, and a dust particle, denoted γ, in Figure 1b. However, many spherulites do not have any observable heterogeneous nucleating agent, and nucleation sites continue to develop throughout the transition, which suggests that there is a combination of homogeneous and heterogeneous nucleation.

The formation of G from the HPL phase also proceeds by nucleation, followed by a radially symmetric growth mechanism. However, the nucleation density of G is usually much lower than that of HPL. This leads to relatively large single crystal G grains consuming multiple smaller HPL grains. The G grain boundaries are distinct from those of the HPL phase, although sometimes common nucleating sites, especially heterogeneous nucleating sites, can be identified both for HPL and the subsequent G grains. The fact that multiple HPL grains combine to form a single G grain reflects the slow nucleation of G, rather than the absence of an epitaxial relationship between the two phases. This particular transition has previously been found to proceed epitaxially.[3,39−41]

The G → C transition is not the main subject of this paper, but the modes of nucleation and growth as well as the retention of grain boundaries will be discussed briefly in order to contrast with the HPL → G transition. The G → C transition did not occur by a nucleation with symmetric growth mechanism. Typically, it followed two concurrent paths: growth from G grain boundaries and uniform growth within a grain. Formation of C at the grain boundaries is rapid, followed by anisotropic growth into the grain, where C regions grow more rapidly in specific directions. The observation of oriented growth agrees with the previously established observation of an epitaxial relationship in this transition.[4,7,40,42,43] The C phase also forms uniformly throughout the grain at a slower rate. This is most likely caused by nucleation and oriented growth on a scale smaller than the microscope resolution, which is several microns. One interesting aspect of the G → C transition is that the grain boundaries established in the G formation are preserved upon conversion to C, as illustrated in Figure 1f,h. The outline of a C grain clearly visible in Figure 1h is redrawn in Figure 1f. The establishment of G grain boundaries could be observed midway through the transition, as grain impingement begins. The G grain of interest (the one corresponding to the dashed outline of Figure 1f) impinges on surrounding grains initially in Figure 1e and also later in Figure 1f. The location of this G grain boundary matches the subsequent observed C grain boundary. This demonstrates that the G and subsequent C share the same grain boundaries.

SAXS. While POM can provide a good deal of information about the phase transitions, it is not sufficient to identify the particular isotropic and anisotropic phases. SAXS was therefore used to confirm phase assignments and transition temperatures. Azimuthally averaged SAXS measurements of SI(22−12)/DEP showed that a DIS SAXS profile converts to a G profile (shown in Figure 2a) within 20 min after a quench from 180 to 153 °C. The DIS scattering profile is characterized by a single broad peak without any higher order peaks, whereas the G phase exhibits a $q^*:\sqrt{4/3}q^*$ ratio of peak positions. These findings are consistent with the interpretation of the POM data. Specifically, the isotropic phases observed by POM in parts a and g of Figure 1 are distinct and correspond to DIS and G, respectively. Detailed kinetic information could not be obtained with SAXS since the requisite measurement times (5 min exposures) were too long relative to the transition times (typically, 5−20 min). The profile of Figure 2a shows G formation occurring, but also there is a subtle peak at $2q^*$ which does not persist into the fully formed G profile (t = 10−20 min). Although this is consistent with transient presence of HPL, it does not provide conclusive identification. However, this characterization and previous extensive studies using SAXS and rheology on similar samples[4,7,30] strongly indicate that this is indeed HPL.

Furthermore, SAXS measurements were used to confirm that the radially expanding G regions during the transition were large single G grains and not polycrystalline G regions. Measurements on SI(22−12)/DEP after shallow quenches yielded very "spotty" SAXS profiles (Figure 2b), whereas deeper quenches had a more isotropic azimuthal behavior (Figure 2c). The "spotty" behavior in Figure 2b suggests that the X-ray beam was scattered by only a few large grains. Since the beam passed through a sample thickness of ca. 1.5 mm, the SAXS image is consistent with the interpretation from the shallow quench POM image (Figure 2d) that the G grains are several hundred micrometers in diameter. In addition, comparison of shallow and deeper quench SAXS profiles (Figure 2, b and c, respectively) demonstrates qualitatively that the shallow quenches result in larger G grains than the deep quenches (i.e., increased isotropic azimuthal behavior corresponds to smaller grains). If the G grains were actually polycrystalline, the patterns would be expected to be the same under both conditions.

Growth Fronts. Since POM measurements capture real-time 2-D images of the samples, it is possible to measure growth front velocities of individual grains. Growth front velocities of G grains were measured in all six samples. In all cases the growth fronts progressed over time at a constant rate. Furthermore, for a given sample and quench temperature, the growth front velocities of all the grains measured were in good agreement. This was especially true for shallow quenches because there was little grain overlap, which allowed ample time for unperturbed grain growth and very accurate measurements of the growth front velocity. An example of a growth front measurement for a shallow quench is presented in Figures 3 and 4. Figure 3 shows POM images from SI(22−12)/DEP quenched to 155 °C at a fixed resolution and field of view. Growth fronts of two grains progressed over time through the field of view, along the direction indicated by the arrows. The growth front displacement is plotted versus time in Figure 4, giving an average growth front velocity of 39.2 μm/min for the two grains. Determination of grain boundaries was not as straightforward for deeper

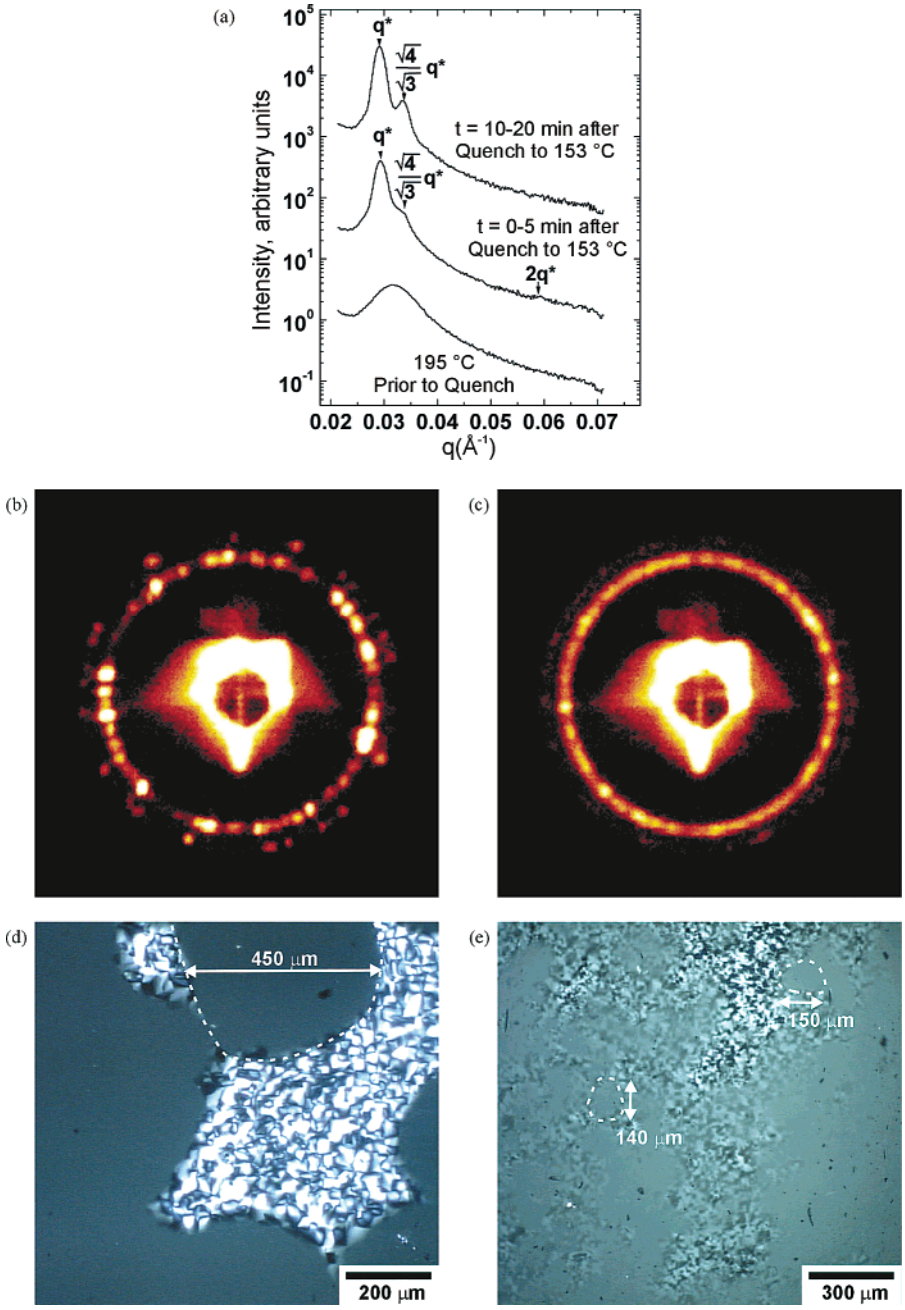

Figure 2. (a) Plot of I vs q for a measurement of SI(22−12) $\phi = 0.7$ in DEP before and after a temperature quench to 153 °C. The ratios of the peak positions verify that the isotropic phase during transition is correctly assigned as G. Also, there is a faint transient $2q^*$ peak for $t = 0-5$ min, which would be expected by the transient presence of HPL. 2-D SAXS images of SI(22−12) $\phi = 0.7$ DEP after quenching to (b) 153 and (c) 148 °C. The spotty pattern indicated fewer grains were in the beam pathway. This corresponds to the POM data. (d) Quenching to 153 °C produced a small number of large grains. (e) Quenching to 148 °C results in a higher density of small grains.

quenches. The POM sample thicknesses were ca. 100 μm, and therefore when the nucleation density was high, the grains were superimposed (e.g., see Figure 2e). It was therefore not always possible to identify distinct growth fronts. On the other hand, the low nucleation rates of the shallow quenches led to grain sizes larger than the sample thickness. The resulting confinement of the growth to two dimensions did not have any observable effect on the growth rates. The growth front velocities that were measured at several quench temperatures for each sample are presented in Figure 5a−f. The error bars for data points in Figure 5 indicate the agreement among the measured growth front velocities; the growth fronts of at least five grains were measured for each sample at each temperature.

Theoretical Predictions. The smooth curves drawn in Figures 5 are the predictions of a relation proposed by Goveas and Milner:[29]

$$\nu \approx \frac{\langle h^2 \rangle^{1/2} N}{\tau_1} [\chi - \chi_{OOT}] g(f) \alpha \qquad (1)$$

where ν is the grain growth front velocity, $\langle h^2 \rangle^{1/2}$ is the root-mean-square end-to-end distance of the chain, N is the degree of polymerization, τ_1 is the polymer chain relaxation time, $g(f)$ is a constant dependent only on the block composition, α is an adjustable scaling parameter, and $(\chi - \chi_{OOT})$ is the difference between the interaction parameters at the quench temperature and the associ-

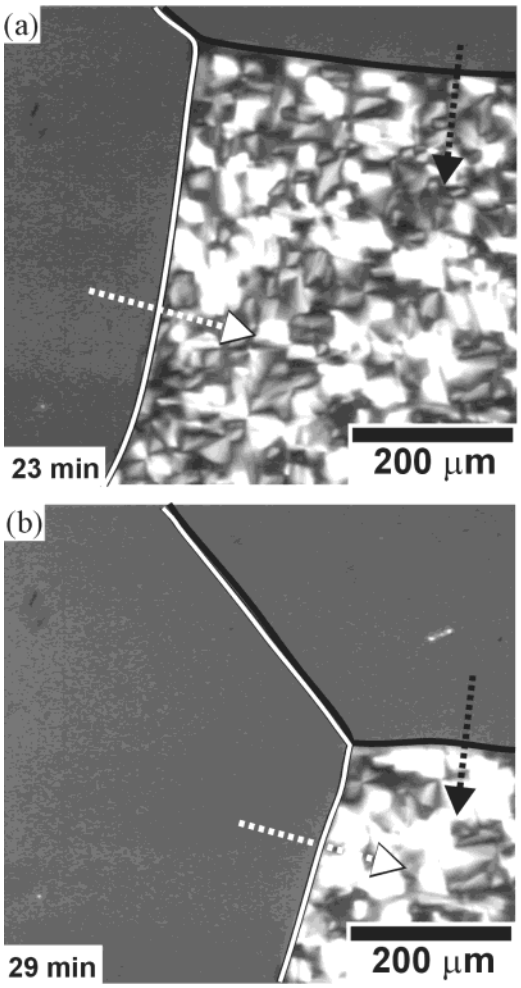

Figure 3. Example of growth front progression over time for HPL to G in SI(22−12) $\phi = 0.7$ in DEP. The two G grains in the images are outlined with white and black lines for clarity, and the corresponding arrows indicate the direction of grain growth.

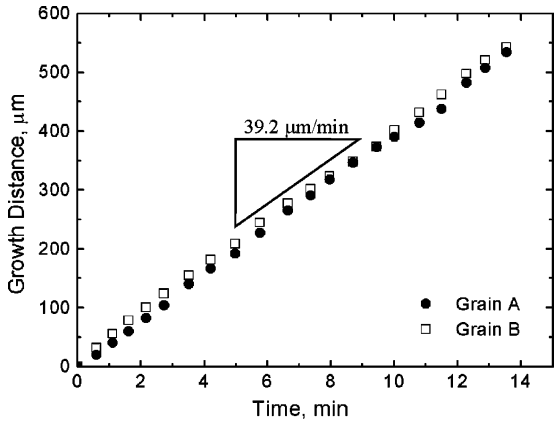

Figure 4. Quantification of growth front velocities for SI(22−12) $\phi = 0.70$ in DEP after a temperature quench to 155 °C. Time and growth distance are zeroed to the first measurement, which occurred during the growth process (i.e., $t = 0 > t_{\text{nucleation}}$). Grain A corresponds to the upper right grain outlined in black in Figure 3, while grain B corresponds to the grain outlined in white.

ated transition T_{OOT}. The value of N was determined from SEC, and $\langle h^2 \rangle^{1/2}$ was estimated using the known statistical segment lengths of PI (6.5 Å) and PS (6.7 Å),[44] while assuming a Gaussian coil conformation. The adjustable scaling factor α was added to the Goveas−Milner equation, for this analysis, to quantify any disagreement between the predicted and experimentally measured values. The $g(f)$ parameter was fixed for all samples to the value of 0.575 reported by Balsara et al.[23] The values of $\langle h^2 \rangle^{1/2}$, N, and α for each of the three samples are listed in Table 1. The parameters $g(f)$, $\langle h^2 \rangle^{1/2}$, N, and α only contribute to the magnitude of ν and not to the temperature dependence.

The parameters that determine the temperature dependence of ν are the difference between the interaction parameters at the quench temperature and the associated transition T_{OOT}, $(\chi - \chi_{OOT})$, and the polymer chain relaxation time, τ_1. Thus, the thermodynamic driving force is embodied in $(\chi - \chi_{OOT})N$, and the chain mobility aspects of the transition are determined by τ_1. As the temperature is lowered further below T_{OOT}, $(\chi - \chi_{OOT})N$ tends to increase ν because of the increasing instability of the parent phase, whereas τ_1 retards ν due to the encroaching glass transition.

Estimates of $(\chi - \chi_{OOT})$ were based on the following function for SI copolymers:[45]

$$\chi_{PS-PI} = \frac{33}{T} - 0.0228 \qquad (2)$$

As there was no T_{OOT} for the HPL → G transition because HPL is not a thermodynamically stable phase, T_{ODT} was used instead. HPL would form only at temperatures below T_{ODT} and was consistently converted to G. Therefore, this apparently "shared T_{ODT}" is a reasonable reference temperature for estimating the relevant difference in χ.

The polymer chain relaxation time, τ_1, could not be determined by measuring the ordered copolymer solutions directly, due to the complicated rheological response of ordered block copolymers. One way to circumvent this would be to access the disordered phase by increasing temperature and then extrapolating back down to the ordered state. However, in this case the required high temperatures led to significant solvent evaporation, and the results were unreliable. Therefore, polystyrene (PS) and polyisoprene (PI) homopolymers of similar molecular weight to the diblocks were measured in the neutral solvent DOP, which has the advantage of being less volatile than the other dialkyl phthalates. Selected measurements were also made in DEP and DBP, and the resulting τ_1 values were in close agreement with the DOP solutions. (The data differed by at most a factor of 2 at all relevant temperatures.) Rheological measurements of PS/DOP and PI/DOP solutions provided full characterization of the terminal and crossover regimes, with good time−temperature superposition. Parts a and b of Figure 6 show the master curves and τ_1 values for PI-22, $\phi = 0.7$, and PS-34, $\phi = 0.7$, respectively. The experimental chain relaxation time, $\tau_{1,exp}$, is taken as the inverse of the frequency where the terminal G' and G'' extrapolations intersect. The master curves were made by shifting the data horizontally around reference temperatures (PS-34 $\phi = 0.7$ DOP: $T_R = 60$ °C; PI-22 $\phi = 0.7$ DOP: $T_R = 0$ °C) and also were slightly vertically shifted to account for density changes. The shift factors, a_T, were fit to the Williams−Landel−Ferry (WLF) equation, which was used to find $\tau_1(T)$, as shown in Figure 7. The diblock $\tau_1(T)$ was determined by scaling the homopolymer values to the correct molecular weight using an $M^{3.4}$ dependence. For example, values for SI(22−12) were scaled to 34 000 g/mol. A weighted mean was made on

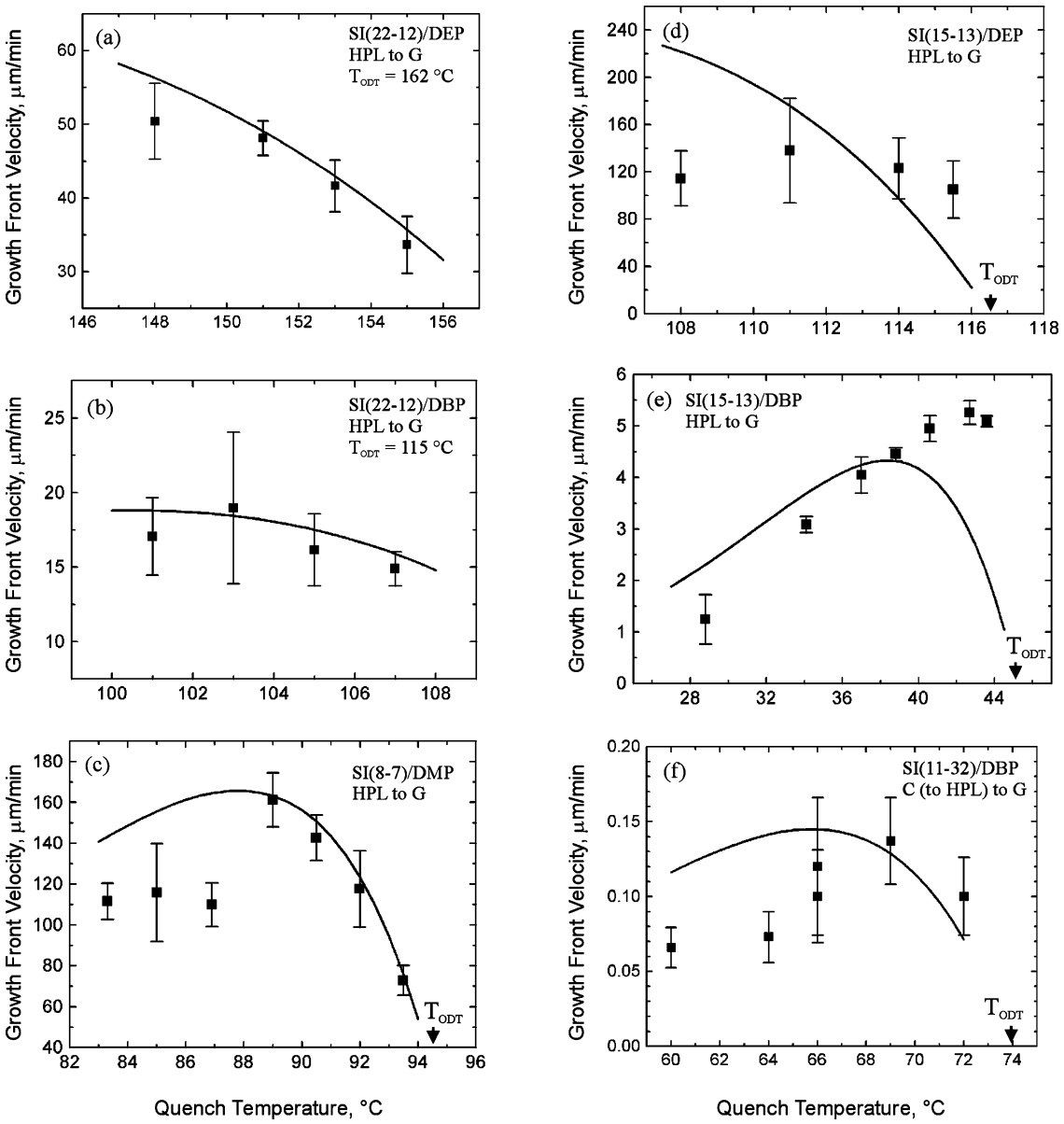

Figure 5. Experimentally measured growth front velocities plotted with the theoretical predictions for (a) SI(22−12) $\phi = 0.70$ in DEP, (b) SI(22−12) $\phi = 0.70$ in DBP, (c) SI(11−32) $\phi = 0.67$ in DBP, (d) SI(8−7) $\phi = 0.70$ in DMP, (e) SI(15−13) $\phi = 0.55$ in DEP, and (f) SI(15−13) $\phi = 0.57$ in DBP.

the basis of eq 3:

$$\tau_{1,SI} = f_{PS}\tau_{1,PS/DOP} + f_{PI}\tau_{1,PI/DOP} \qquad (3)$$

where f is the volume fraction of each block in the given diblock sample and τ_1 is the chain relaxation time of either PS/DOP, PI/DOP, or the SI sample. The calculated diblock relaxation times for SI(11−32)/DBP and the SI(22−12) samples are shown as data points in Figure 7 for the temperatures that were characterized experimentally. The homopolymer solution data are also shown. The homopolymer solutions used for the other samples are listed in Table 2. Since the PI/DOP τ_1 values are significantly lower than the PS/DOP values, the PS/DOP term dominates the predicted SI relaxation time. This is reasonable because the slower PS block is expected to limit the mobility of the entire chain.

Theory−Experiment Comparison. On the whole, there is remarkable agreement between the growth velocities and the predictions of eq 1. First, the presence or absence of a growth rate maximum, and its location, are captured very reliably (with the exception of Figure 5d.) This feature results from the competition between the thermodynamic driving force and the temperature dependence of the chain dynamics. Although the procedures we have adopted to estimate these quantities are necessarily approximate, it appears that these approximations are reasonable. Second, the magnitude of the growth velocity is also in fair agreement with eq 1, as embodied in the parameter α. One should probably be satisfied with an order of magnitude agreement between experiment and theory in this regard, given the many local details that could influence the experimental v. On the other hand, α does vary by a factor of 46 (see Table 1), which suggests that there is more than just a single systematic error at work. We offer a few further comments on the individual solutions, as follows.

SI(22−12)/DEP and SI(22−12)/DBP. SI(22−12)/DEP and SI(22−12)/DBP required α values of 0.1 and 0.25, respectively. The experimental growth front velocities were measured by POM with little uncertainty. The lack of agreement could be caused by systematic

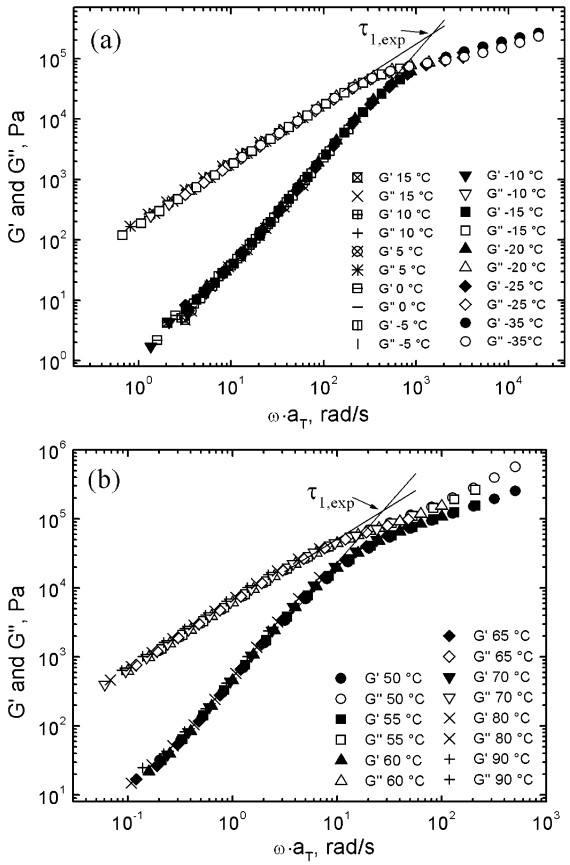

Figure 6. Master curves for (a) PI 22K $\phi = 0.70$ in DOP and (b) PS 34K $\phi = 0.70$ in DOP.

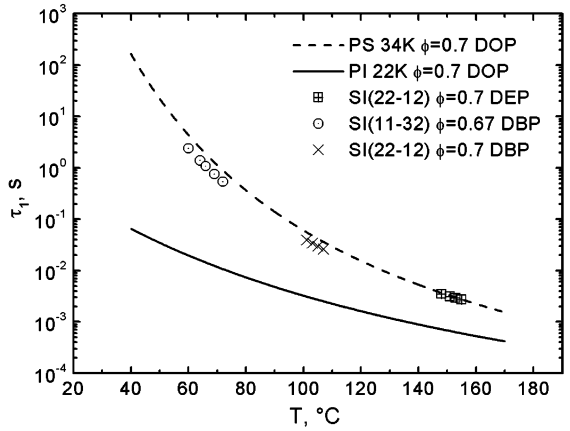

Figure 7. WLF fits to experimental data and calculated relaxation times for the indicated samples.

uncertainties in the parameters comprising the Goveas−Milner equation. For example, the values of $g(f)$ and τ_1 are only estimates because they could not be measured directly. Specifically, $g(f)$ should be slightly different for each polymer, but because of the presence of selective solvent and the metastable nature of the HPL phase, it is not possible to know how $g(f)$ would vary between the samples. The values of τ_1 were estimated with the same method for all the samples, but the SI(22−12) samples could be affected by random error. The high transition temperature of SI(22−12)/DEP was especially susceptible since the rheology measurements needed to be shifted by as much as 100 °C to determine the relaxation times.

SI(11−32)/DBP. SI(11−32)/DBP showed the largest discrepancy between theory and experiment, requiring

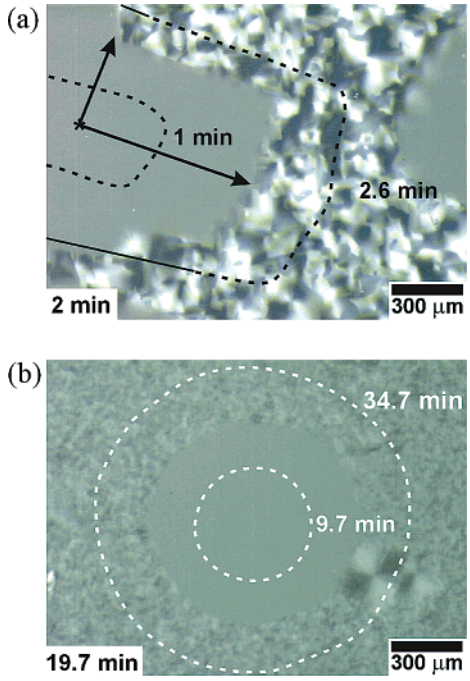

Figure 8. Anisotropic vs isotropic grain growth of G. (a) SI(15−13) in DEP exhibits anisotropic grain growth with an aspect ratio of approximately 1.9. (b) SI(15−13) in DBP shows radially symmetric grain growth. The dashed lines indicate the location of the grain boundary at the indicated times.

an α value of 0.05. A large part of the reason for disagreement is the same as just discussed with the SI(22−12) samples. Another possible factor could be the different phase behavior. Unlike the other samples, which have a DIS → (HPL) → G sequence upon quenching, SI(11−32)/DBP shows a C → (HPL) → G transition sequence upon quenching, with the HPL phase forming in the deeper temperature quenches. Starting with the C phase instead of DIS could influence the value of $g(f)$, which is transition-dependent.

SI(15−13)/DEP. While the magnitude of the growth front velocities in SI(15−13)/DEP showed good agreement between theory and experiment, the dependence on quench temperature did not agree well. In this case the disagreement was most likely caused by difficulties in measuring the growth fronts. Unlike the other samples, the HPL → G transition in SI(15−13)/DEP did not always occur through radially symmetric growth. Figure 8a shows that the forming G grain has an aspect ratio of 1.9, with roughly two perpendicular growth fronts. This is in marked contrast with the radially symmetric growth seen in SI(15−13)/DBP (Figure 8b). Anisotropy of growth was observed in most grains at all quench temperatures for SI(15−13)/DEP. It was very rarely observed in any of the other samples. Therefore, the disagreement in the temperature dependence is likely a consequence of the deviation from the typical radially symmetric grain growth. Also, the anisotropy added uncertainty to the measuring of growth fronts. Because of grain overlap, especially at the lower quench temperatures, the issue of anisotropy could not be consistently quantified and accounted for. This reduces the consistency of observation throughout the quench temperatures, which adds error to the measured temperature dependence.

Summary

Polarized optical microscopy was used to quantify the grain growth rate for the gyroid phase following tem-

perature jumps. Six different styrene−isoprene copolymer solutions were examined, in dialkyl phthalate solvents. In all cases the nonbirefringent gyroid grains emerged from a birefringent, metastable perforated layer precursor. Interestingly, the nucleation of gyroid grains from the perforated layer phase was quite slow, such that individual gyroid "crystallites" consumed many perforated layer grains. Grains grew isotropically, and the fronts moved with a constant velocity. Depending on conditions (e.g., sample, concentration, and temperature), the velocities ranged from 0.06 to 160 μm/min. In some samples the velocity increased with decreasing temperature, indicating the influence of the thermodynamic driving force, whereas in other cases the velocity decreased, suggesting the influence of chain dynamics. The results were compared quantitatively with the theory of Goveas and Milner, using longest relaxation times estimated from rheological measurements. In general, the theory captured the dependence on quench temperature and was also reasonably successful in anticipating the magnitude of the velocity. This application of optical microscopy to block copolymer transition kinetics is shown to be relatively straightforward and capable of providing important visual information about the nature of the growth process as well as quantifying growth rates.

Acknowledgment. This work was supported by the National Science Foundation through Award DMR-9901087.

References and Notes

(1) Bates, F. S.; Fredrickson, G. H. *Annu. Rev. Phys. Chem.* **1990**, *41*, 525−557.
(2) Hamley, I. W. *The Physics of Block Copolymers*; Oxford University Press: Oxford, 1998.
(3) Hajduk, D. A.; Ho, R.-M.; Hillmyer, M. A.; Bates, F. S.; Almdal, K. *J. Phys. Chem. B* **1998**, *102*, 1356−1363.
(4) Wang, C.-Y.; Lodge, T. P. *Macromolecules* **2002**, *35*, 6997−7006.
(5) Qi, S.; Wang, Z.-G. *Phys. Rev. E* **1997**, *55*, 1682−1697.
(6) Qi, S.; Wang, Z.-G. *Macromolecules* **1997**, *30*, 4491−4497.
(7) Wang, C.-Y.; Lodge, T. P. *Macromol. Rapid Commun.* **2002**, *23*, 49−54.
(8) Wang, Z.-G. *Curr. Opin. Colloid Interface Sci.* **1998**, *3*, 428−435.
(9) Floudas, G.; Ulrich, R.; Wiesner, U. *J. Chem. Phys.* **1999**, *110*, 652−663.
(10) Krishnamoorti, R.; Modi, M. A.; Tse, M. F.; Wang, H. C. *Macromolecules* **2000**, *33*, 3810−3817.
(11) Sakurai, S.; Umeda, H.; Taie, K.; Nomura, S. *J. Chem. Phys.* **1996**, *105*, 8902−8908.
(12) Sakurai, S.; Umeda, H.; Furukawa, C.; Irie, H.; Nomura, S.; Hyun Lee, H.; Kon Kim, J. *J. Chem. Phys.* **1998**, *108*, 4333−4339.
(13) Imai, M.; Saeki, A.; Teramoto, T.; Kawaguchi, A.; Nakaya, K.; Kato, T.; Ito, K. *J. Chem. Phys.* **2001**, *115*, 10525−10531.
(14) Jeong, U.; Lee, H. H.; Yang, H.; Kim, J. K.; Okamoto, S.; Aida, S.; Sakurai, S. *Macromolecules* **2003**, *36*, 1685−1693.
(15) Rosedale, J. H.; Bates, F. S. *Macromolecules* **1990**, *23*, 2329−2338.
(16) Singh, M. A.; Harkless, C. R.; Nagler, S. E.; Shannon, R. F.; Ghosh, S. S. *Phys. Rev. B*: *Condens. Matter* **1993**, *47*, 8425−8435.
(17) Adams, J. L.; Quiram, D. J.; Graessley, W. W.; Register, R. A.; Marchand, G. R. *Macromolecules* **1996**, *29*, 2929−2938.
(18) Hajduk, D. A.; Tepe, T.; Takenouchi, H.; Tirrell, M.; Bates, F. S.; Almdal, K.; Mortensen, K. *J. Chem. Phys.* **1998**, *108*, 326−333.
(19) Kim, J. K.; Lee, H. H.; Ree, M.; Lee, K.-B.; Park, Y. *Macromol. Chem. Phys.* **1998**, *199*, 641−653.
(20) Sakamoto, N.; Hashimoto, T. *Macromolecules* **1998**, *31*, 3292−3302.
(21) Pan, L. H.; Singh, M. A.; Salomons, G. J.; Gupta, J. A.; Capel, M. S. *J. Macromol. Sci., Phys.* **1996**, *B35*, 749−761.
(22) Kim, W. G.; Garetz, B. A.; Newstein, M. C.; Balsara, N. P. *J. Polym. Sci., Part B*: *Polym. Phys.* **2001**, *39*, 2231−2242.
(23) Balsara, N. P.; Garetz, B. A.; Chang, M. Y.; Dai, H. J.; Newstein, M. C.; Goveas, J. L.; Krishnamoorti, R.; Rai, S. *Macromolecules* **1998**, *31*, 5309−5315.
(24) Kim, W. G.; Chang, M. Y.; Garetz, B. A.; Newstein, M. C.; Balsara, N. P.; Lee, J. H.; Hahn, H.; Patel, S. S. *J. Chem. Phys.* **2001**, *114*, 10196−10211.
(25) Dai, H. J.; Balsara, N. P.; Garetz, B. A.; Newstein, M. C. *Phys. Rev. Lett.* **1996**, *77*, 3677−3680.
(26) Newstein, M. C.; Garetz, B. A.; Balsara, N. P.; Chang, M. Y.; Dai, H. J. *Macromolecules* **1998**, *31*, 64−76.
(27) Balsara, N. P.; Garetz, B. A.; Newstein, M. C.; Bauer, B. J.; Prosa, T. J. *Macromolecules* **1998**, *31*, 7668−7675.
(28) Wang, H.; Newstein, M. C.; Chang, M. Y.; Balsara, N. P.; Garetz, B. A. *Macromolecules* **2000**, *33*, 3719−3730.
(29) Goveas, J. L.; Milner, S. T. *Macromolecules* **1997**, *30*, 2605−2612.
(30) Lodge, T. P.; Pudil, B.; Hanley, K. J. *Macromolecules* **2002**, *35*, 4707−4717.
(31) Hanley, K. J.; Lodge, T. P. *J. Polym. Sci., Part B*: *Polym. Phys.* **1998**, *36*, 3101−3113.
(32) Hanley, K. J.; Lodge, T. P.; Huang, C.-I. *Macromolecules* **2000**, *33*, 5918−5931.
(33) Sawyer, L. C.; Grubb, D. T. *Polymer Microscopy*, 2nd ed.; Chapman & Hall: New York, 1996.
(34) Hemsley, D. A. *Applied Polymer Light Microscopy*; Elsevier Applied Science: New York, 1989.
(35) Hashimoto, T.; Wang, W. *Polymer* **2000**, *41*, 4729.
(36) Foerster, S.; Berton, B.; Hentze, H. P.; Kraemer, E.; Antonietti, M.; Lindner, P. *Macromolecules* **2001**, *34*, 4610−4623.
(37) Wittmann, J. C.; Lotz, B.; Candau, F.; Kovacs, A. J. *J. Polym. Sci., Part B*: *Polym. Phys.* **1982**, *20*, 1341−1353.
(38) Kimishima, K.; Koga, T.; Hashimoto, T. *Macromolecules* **2000**, *33*, 968−977.
(39) Foerster, S.; Khandpur, A. K.; Zhao, J.; Bates, F. S.; Hamley, I. W.; Ryan, A. J.; Bras, W. *Macromolecules* **1994**, *27*, 6922−6935.
(40) Schulz, M. F.; Bates, F. S.; Almdal, K.; Mortensen, K. *Phys. Rev. Lett.* **1994**, *73*, 86−89.
(41) Vigild, M. E.; Almdal, K.; Mortensen, K.; Hamley, I. W.; Fairclough, J. P. A.; Ryan, A. J. *Macromolecules* **1998**, *31*, 5702−5716.
(42) Clerc, M.; Levelut, A. M.; Sadoc, J. F. *J. Phys. II* **1991**, *1*, 1263−1276.
(43) Rancon, Y.; Charvolin, J. *J. Phys. Chem.* **1988**, *92*, 2646−2651.
(44) Fetters, L. J.; Lohse, D. J.; Richter, D.; Witten, T. A.; Zirkel, A. *Macromolecules* **1994**, *27*, 4639−4647.
(45) Lodge, T. P.; Pan, C.; Jin, X.; Liu, Z.; Zhao, J.; Maurer, W. W.; Bates, F. S. *J. Polym. Sci., Part B*: *Polym. Phys.* **1995**, *33*, 2289−2293.

MA034833W